Convolution of multifractals and the local magnetization in a random-field Ising chain

2001 J. Phys. A: Math. Gen. 34 8057

(http://iopscience.iop.org/0305-4470/34/39/308)

INSTITUTE OF PHYSICS PUBLISHING JOURNAL OF PHYSICS A: MATHEMATICAL AND GENERAL

J. Phys. A: Math. Gen. **34** (2001) 8057–8079 PII: S0305-4470(01)22205-7

Convolution of multifractals and the local magnetization in a random-field Ising chain

Thomas Nowotny and Ulrich Behn

Institut für Theoretische Physik, Universität Leipzig, Augustusplatz 10, 04109 Leipzig, Germany

Received 21 February 2001, in final form 16 July 2001
Published 21 September 2001
Online at stacks.iop.org/JPhysA/34/8057

Abstract

The local magnetization in the one-dimensional random-field Ising model is essentially the sum of two effective fields with multifractal probability measure. The probability measure of the local magnetization is thus the convolution of two multifractals. In this paper we prove relations between the multifractal properties of two measures and the multifractal properties of their convolution. The pointwise dimension at the boundary of the support of the convolution is the sum of the pointwise dimensions at the boundary of the support of the convoluted measures and the generalized box dimensions of the convolution are bounded from above by the sum of the generalized box dimensions of the convoluted measures. The generalized box dimensions of the convolution of Cantor sets with weights can be calculated analytically for certain parameter ranges and illustrate effects we also encounter in the case of the measure of the local magnetization. Returning to the study of this measure we apply the general inequalities and present numerical approximations of the D_q-spectrum. For the first time we are able to obtain results on multifractal properties of a physical quantity in the one-dimensional random-field Ising model which in principle could be measured experimentally. The numerically generated probability densities for the local magnetization show impressively the gradual transition from a monomodal to a bimodal distribution for growing random field strength h.

PACS numbers: 05.45.Df, 05.50.+q, 75.10.Nr, 05.70.Fh

1. Introduction

Multifractal measures appear in a variety of contexts. The one-dimensional random-field Ising models [1–20] and random-exchange [21–23] Ising models as well as other one-dimensional disordered systems [24–27], Bernoulli convolutions [28] and even learning in neural networks [29–31] are prominent examples. The use of a reduction scheme for the partition function of the one-dimensional random-field Ising model first introduced by

Ruján [10] results in the partition function of a one-spin system in an effective field (one-sided reduction, spin at the boundary) [4–16] or in two effective fields (two-sided reduction, spin in the bulk) [17], which is the appropriate point of view when investigating the local magnetization. The effective fields are governed by an iteration, thus giving rise to a random iterated function system (RIFS), which is known to have a unique invariant measure [32]. The invariant measure of the effective fields is typically a multifractal [1, 4, 6].

In a recent publication [9] phase transitions in the D_q-spectrum of this invariant measure of the effective field were investigated (cf also [11, 12]) and tight bounds on the D_q based on the pointwise dimension at specific points generalizing results in [13] were formulated. The combination of the two allows a more or less complete understanding of the D_q-spectrum of the invariant measure of the effective field by exclusively analytical methods. Naturally the question arises of whether these results are relevant for physical quantities such as correlation functions or the local magnetization, which in principle are experimentally accessible.

The local magnetization can be expressed as a function of the effective fields [4–6] and we show in this paper that a considerable amount of the knowledge of the multifractal properties of the invariant measure of the effective field can be transferred to the measure of the local magnetization. Being essentially the sum of two effective fields with multifractal probability measure the local magnetization has a probability measure which is the convolution of two multifractal measures. We therefore first prove general relations between the multifractal properties of two measures and the multifractal properties of their convolution, which then can be applied to the random-field Ising chain. As the convolution of measures is the composition of constructing the product measure and projecting it in a certain way, the work on projections of multifractal (product) measures [33, 34] is related to our subject. Whereas these papers focus mainly on properties of projected measures with respect to typical projections, we are here concerned with a given projection leading to the convolution. This special case need not necessarily have the properties of a generic projection. There is also related work on the superposition of multifractals [35–37] and some remarks on the convolution of multifractals in [38].

In addition to the mathematical results we also calculate the measure of the local magnetization and its multifractal spectrum numerically. Random-field Ising systems can be realized as dilute antiferromagnets in uniform magnetic fields [39] and the local magnetization can in principle be measured by neutron scattering or Mößbauer spectroscopy. The probability distribution of the local magnetization with respect to the disorder therefore should be experimentally accessible and could be compared with our numerical results presented in figure 9. Especially the gradual transition from a strongly peaked monomodal distribution to a strongly peaked bimodal distribution observed numerically should clearly be visible. Depending on the quality of the measurement it is even feasible to calculate the D_q-spectrum of the obtained probability distribution by the box methods described in section 5 and to compare to the results presented here. This should at least reproduce the general form of the multifractal spectrum shown in figure 7.

The paper is organized as follows. After recalling the model and the reduction scheme in section 2 we prove general bounds on the D_q-spectrum of the convolution of two measures and relations between certain pointwise dimensions in section 3. The results are applied to the situation of the local magnetization in the random-field Ising chain. We then explicitly calculate some D_q-spectra in the simplified situation of the convolution of equal-scale Cantor sets with weights in section 4. In section 5 we present numerical results for the D_q-spectrum of the measure of the local magnetization and in the concluding section 6 we summarize our results and draw some conclusions.

2. The model

In the following we consider the one-dimensional random-field Ising model with quenched disorder which for N spins has the Hamiltonian

$$H_N(\{s\}_N) = -J\sum_{i=a}^{b-1} s_i s_{i+1} - \sum_{i=a}^{b} h_i s_i \tag{2.1}$$

with $a < 0 < b$ and $b - a + 1 = N$. s_i denotes the classical spins at site i of the chain taking values ± 1, J is the coupling strength between spins and h_i is the random field at site i. The random fields are independent identically distributed random variables with probability density

$$\rho(h_i) = \tfrac{1}{2}\delta(h_i - h) + \tfrac{1}{2}\delta(h_i + h) \qquad h \in \mathbb{R}^+. \tag{2.2}$$

In former work we used a reformulation of the canonical partition function $Z_N = \sum_{\{s\}_n} \exp(-\beta H_N(\{s\}_N))$ to the partition function of the spin s_a at the left-hand boundary of the chain in an effective field $x_a^{(N)}$, which was first introduced by Ruján [10],

$$Z_N = \sum_{s_a=\pm 1} \exp\left(\beta\left[x_a^{(N)} s_a + \sum_{i=a+1}^{b} B(x_i^{(N)})\right]\right) \tag{2.3}$$

$$x_i^{(N)} = A(x_{i+1}^{(N)}) + h_i \qquad x_{b+1}^{(N)} = 0 \tag{2.4}$$

with

$$A(x) = (2\beta)^{-1}\ln(\cosh\beta(x+J)/\cosh\beta(x-J)) \tag{2.5}$$

$$B(x) = (2\beta)^{-1}\ln(4\cosh\beta(x+J)\cosh\beta(x-J)). \tag{2.6}$$

When viewing (2.4) as a RIFS we will also write x_n instead of $x_i^{(N)}$ for the effective field after $n = N - i + 1$ iterations of (2.4). The effective fields x_n are random variables on the random-field probability space and we write $p_n(x)$ for their induced probability density, $P_n(x) = \int_0^x p_n(\xi)\,\mathrm{d}\xi$ for their distribution function and $\mu_n(X) = \int_X p_n$ for their measures. The iteration (2.4) induces a Frobenius–Perron (Chapman–Kolmogorov) equation for the distribution functions,

$$P_n(x) = \int \mathrm{d}h\,\rho(h) P_{n-1}\big(A^{-1}(x-h)\big) = \sum_{\sigma=\pm}\tfrac{1}{2}P_{n-1}\big(f_\sigma^{-1}(x)\big) \tag{2.7}$$

and accordingly for the densities and measures. The symbols $f_\pm$ denote the functions $f_\pm(x) := A(x) \pm h$. The Frobenius–Perron equation has a unique invariant measure $\mu^{(x)}$ and the measures $\mu_n^{(x)}$ converge to $\mu^{(x)}$ in the weak topology of Borel measures on $\mathbb{R}$. The invariant measure $\mu^{(x)}$ therefore is the measure of the effective field x in the thermodynamic limit $b \to \infty$ ($n \to \infty$ in the notation of the RIFS).

In this paper we focus our interest on the local magnetization in the bulk which is given by $m_{i,N}^{\mathrm{bulk}} = \langle s_i\rangle_N$ at some site $a < i < b$ inside the chain. To obtain $\langle s_i\rangle_N$ we rewrite the partition function to a one-spin partition function with remaining spin s_i,

$$Z_N = \sum_{s_i=\pm 1} \exp\left(\beta\left[\big(x_i^{(N)} + A(y_{i-1}^{(N)})\big)s_i + \sum_{j=a}^{i-1} B(y_j^{(N)}) + \sum_{j=i+1}^{b} B(x_j^{(N)})\right]\right) \tag{2.8}$$

with two effective fields

$$x_j^{(N)} = A(x_{j+1}^{(N)}) + h_j \qquad i \leqslant j \leqslant b \qquad x_{b+1}^{(N)} = 0 \tag{2.9}$$

$$y_j^{(N)} = A(y_{j-1}^{(N)}) + h_j \qquad a \leqslant j < i \qquad y_{a-1}^{(N)} = 0 \tag{2.10}$$

from the right and the left of site i respectively. The local magnetization at i is thus given by [4–6]

$$m_{i,N}^{\text{bulk}} = \langle s_i \rangle_N = \tanh \beta\big(x_i^{(N)} + A(y_{i-1}^{(N)})\big). \tag{2.11}$$

Let us introduce the notation

$$f_{\#}(\mu)(X) := \mu(f^{-1}(X)) \tag{2.12}$$

for the mapping on Borel measures induced by a measurable function f, for example $\tanh \beta_{\#}(\mu)(X) = \mu(1/\beta \operatorname{artanh}(X))$. For the measure of $m_{i,N}^{\text{bulk}}$ we obtain in this notation

$$\mu_{l,r}^{(m)} = \tanh \beta_{\#}(\mu_l^{(x)} * A_{\#}\mu_r^{(y)}) \tag{2.13}$$

with $l = i - a - 1$ and $r = b - i$. As the effective fields share the same Frobenius–Perron equation (2.7) and the invariant measure of this equation is unique, the measures $\mu^{(x)}$ of the right-hand effective field in the thermodynamic limit $b \to \infty$ and $\mu^{(y)}$ of the left-hand effective field in the thermodynamic limit $a \to -\infty$ are identical. Therefore, as we will see below, the measure $\mu_{l,r}^{(m)}$ of the local magnetization in the bulk converges to

$$\mu^{(m)} = \tanh \beta_{\#}(\mu^{(x)} * A_{\#}\mu^{(x)}) \tag{2.14}$$

in the thermodynamic limit $a \to -\infty$, $b \to \infty$ (cf lemma 3.1 below), i.e. the local magnetization $m_{i,N}^{\text{bulk}}$ converges in distribution to a random variable m^{bulk} with measure $\mu^{(m)}$. Please note that $\mu^{(m)}$ is space independent because of the uniqueness of the invariant measure of the Frobenius–Perron equation and the continuity of the convolution.

The local magnetization *at the boundary* on the other hand is obtained if we consider only one effective field, i.e.

$$m^{\text{boundary}} = \langle s_a \rangle = \tanh \beta x \tag{2.15}$$

which has the measure $\tanh \beta_{\#}\mu^{(x)}$. The multifractal properties of $\mu^{(x)}$ are well known (cf [9,11]) and general arguments show that $\tanh \beta_{\#}$ has no effect on the D_q-spectrum (cf [40]) such that the results apply to the measure of m^{boundary} as well. The main point of this paper is the generalization to the magnetization of the bulk, which is of greater physical interest.

3. Convolution of multifractals

In this section $(\mu_n)_{n\in\mathbb{N}}$ and $(\nu_n)_{n\in\mathbb{N}}$ denote sequences of bounded Borel measures on $\mathbb{R}$ which are Cauchy sequences with respect to the Hutchinson metric d_{Hutch} (cf [32]). As the space of bounded Borel measures on $\mathbb{R}$ is complete with respect to d_{Hutch} [32], (μ_n) and (ν_n) converge and we write $\mu := d_{\text{Hutch}}\text{-lim}_{n\to\infty}\, \mu_n$ and $\nu := d_{\text{Hutch}}\text{-lim}_{n\to\infty}\, \nu_n$. As explained above we are interested in the properties of the convolution of bounded Borel measures. The convolution of two bounded Borel measures μ and ν is always well defined (cf [41]) and will in the following be denoted by $\mu * \nu$. As a first step we show that the convolution is continuous with respect to d_{Hutch}.

Lemma 3.1 (Continuity of the convolution). *Let $(m_i)_{i\in\mathbb{N}}$ and $(n_i)_{i\in\mathbb{N}}$ be two monotonically growing unbounded sequences of natural numbers. Then $(\mu_{m_i} * \nu_{n_i})_{i\in\mathbb{N}}$ converges to a bounded Borel measure in Hutchinson topology and the limit is $d_{\text{Hutch}}\text{-lim}_{i\to\infty}\, \mu_{m_i} * \nu_{n_i} = \mu * \nu$.*

Proof. Let $\varepsilon > 0$. The convergence of $(\mu_n)_{n\in\mathbb{N}}$ and $(\nu_n)_{n\in\mathbb{N}}$ implies the existence of numbers $M, N \in \mathbb{N}$ such that for all $i \geqslant M$ $d_{\text{Hutch}}(\mu_{m_i}, \mu) \leqslant \varepsilon$ and for all $i \geqslant N$ $d_{\text{Hutch}}(\nu_{n_i}, \nu) \leqslant \varepsilon$. Let $\tilde{N} := \max(M, N)$. For all $i \geqslant \tilde{N}$ we then have

$$d_{\text{Hutch}}(\mu_{m_i} * \nu_{n_i}, \mu * \nu) = \sup\left\{ \int f(z)\, \mu_{m_i} * \nu_{n_i}(\mathrm{d}z) - \int f(z)\, \mu * \nu(\mathrm{d}z) \;\middle|\; \operatorname{Lip}(f) \leqslant 1 \right\}. \tag{3.1}$$

The definition of the convolution of two measures implies $\int f(z)\,\mu_{m_i} * \nu_{n_i}(\mathrm{d}z) = \iint f(x+y)\mu_{m_i}(\mathrm{d}x)\nu_{n_i}(\mathrm{d}y)$ and $\int f(z)\,\mu*\nu(\mathrm{d}z) = \iint f(x+y)\mu(\mathrm{d}x)\nu(\mathrm{d}y)$. Inserting $0 = -\iint f(x+y)\mu(\mathrm{d}x)\nu_{n_i}(\mathrm{d}y) + \iint f(x+y)\nu_{n_i}(\mathrm{d}y)\mu(\mathrm{d}x)$ we obtain

$$
\begin{aligned}
&d_{\mathrm{Hutch}}(\mu_{m_i} * \nu_{n_i}, \mu * \nu) \\
&\quad = \sup\left\{ \int \left(\int f(x+y)\mu_{m_i}(\mathrm{d}x) - \int f(x+y)\mu(\mathrm{d}x) \right)\nu_{n_i}(\mathrm{d}y) \right. \\
&\qquad \left. + \int \left(\int f(x+y)\nu_{n_i}(\mathrm{d}y) - \int f(x+y)\nu(\mathrm{d}y) \right)\mu(\mathrm{d}x) \;\middle|\; \mathrm{Lip}(f) \leqslant 1 \right\} \qquad (3.2) \\
&\quad \leqslant \int \sup\left\{ \int f(x+y)\mu_{m_i}(\mathrm{d}x) - \int f(x+y)\mu(\mathrm{d}x) \;\middle|\; \mathrm{Lip}(f) \leqslant 1 \right\}\nu_{n_i}(\mathrm{d}y) \\
&\qquad + \int \sup\left\{ \int f(x+y)\nu_{n_i}(\mathrm{d}y) - \int f(x+y)\nu(\mathrm{d}y) \;\middle|\; \mathrm{Lip}(f) \leqslant 1 \right\}\mu(\mathrm{d}x). \qquad (3.3)
\end{aligned}
$$

As the condition $\mathrm{Lip}(f) \leqslant 1$ is translationally invariant we further obtain

$$
\begin{aligned}
&\sup\left\{ \int f(x+y)\mu_{m_i}(\mathrm{d}x) - \int f(x+y)\mu(\mathrm{d}x) \;\middle|\; \mathrm{Lip}(f) \leqslant 1 \right\} \\
&\qquad = \sup\left\{ \int f(x)\mu_{m_i}(\mathrm{d}x) - \int f(x)\mu(\mathrm{d}x) \;\middle|\; \mathrm{Lip}(f) \leqslant 1 \right\} \\
&\qquad = d_{\mathrm{Hutch}}(\mu_{m_i}, \mu) \leqslant \varepsilon. \qquad (3.4)
\end{aligned}
$$

In the same way

$$
\sup\left\{ \int f(x+y)\nu_{n_i}(\mathrm{d}y) - \int f(x+y)\nu(\mathrm{d}y) \;\middle|\; \mathrm{Lip}(f) \leqslant 1 \right\} = d_{\mathrm{Hutch}}(\nu_{n_i}, \nu) \leqslant \varepsilon. \qquad (3.5)
$$

We thus arrive at

$$
d_{\mathrm{Hutch}}(\mu_{m_i} * \nu_{n_i}, \mu * \nu) \leqslant \int \varepsilon\,\nu_{n_i}(\mathrm{d}y) + \int \varepsilon\,\mu(\mathrm{d}x) = (\|\nu_{n_i}\| + \|\mu\|)\,\varepsilon \qquad (3.6)
$$

in which $\|\nu_{n_i}\| = \nu_{n_i}(\mathbb{R})$ and $\|\mu\| = \mu(\mathbb{R})$ denote the total mass of ν_{n_i} and μ respectively. □

As the metric d_{Hutch} topology and the weak topology coincide on bounded Borel measures with compact support [32] we have the following corollary.

Corollary 3.2. *If* supp μ *and* supp ν *are compact,* $w\text{-}\lim_{i\to\infty} \mu_{m_i} * \nu_{n_i} = \mu * \nu$. *Furthermore* supp $\mu * \nu$ *is also compact.*

For the situation of the two-sided random-field Ising chain considered in this paper lemma 3.1 implies that the thermodynamic limit $l, r \to \infty$ can be carried out in an arbitrary way and that the result is the same as when first taking the thermodynamic limit for the effective fields and then calculating the measure of the local magnetization. Having detailed knowledge of the properties of the D_q-spectrum and the pointwise dimensions of the invariant measure of the effective field it is now interesting to investigate the relationship of the D_q-spectra and pointwise dimensions of μ and ν to the D_q-spectrum and pointwise dimensions of $\mu * \nu$. The following lemmata allow us to transfer the knowledge about the multifractal properties of the invariant measure of the effective field gathered in [9] to the measure of the local magnetization. In the following we consider only measures with bounded, i.e. compact support. Let $x_- := \min \mathrm{supp}\,\mu > -\infty$ denote the left and $x_+ := \max \mathrm{supp}\,\mu < \infty$ the right boundary of supp μ. For the boundaries of supp ν we write y_- and y_+. The pointwise dimension at the boundary of the support of $\mu*\nu$ can be obtained from the pointwise dimensions at x_+, x_-, y_+ and y_-.

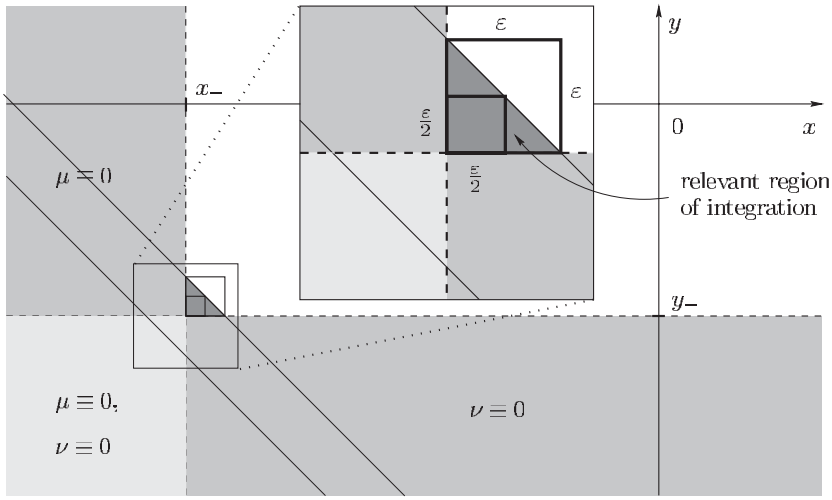

Figure 1. Illustration of the proof of lemma 3.3. The diagonal strip is the region in which $\mathbf{1}_{B_\varepsilon(z_-)}(x+y)$ is non-zero. Therefore, the dark grey triangle is the relevant region with non-zero contributions to the integral (3.8). As μ and ν are positive measures, integration over the small square of side length $\frac{\varepsilon}{2}$ provides a lower and integration over the larger square of side length ε an upper bound on the integral.

Lemma 3.3 (Pointwise dimension of $\mu * \nu$ at the boundary of its support). *The left-hand boundary of $\mu * \nu$ is $z_- = x_- + y_-$ and the pointwise dimension $D_p(z_-; \mu * \nu) = D_p(x_-; \mu) + D_p(y_-; \nu)$. The result for the right-hand boundary is analogous.*

Proof. The pointwise dimension of $\mu * \nu$ at z_- is defined as

$$D_p(z_-; \mu * \nu) = \lim_{\varepsilon \to 0} \frac{\ln(\mu * \nu(B_\varepsilon(z_-)))}{\ln \varepsilon} \tag{3.7}$$

in which $\mu * \nu(B_\varepsilon(z_-))$ is given by

$$\mu * \nu(B_\varepsilon(z_-)) = \iint \mathbf{1}_{B_\varepsilon(z_-)}(x+y)\mu(\mathrm{d}x)\nu(\mathrm{d}y). \tag{3.8}$$

The symbol $\mathbf{1}_X$ denotes the characteristic function of a set X, i.e. $\mathbf{1}_X(x) = 1$ if $x \in X$ and $= 0$ otherwise. The area in which $\mathbf{1}_{B_\varepsilon(z_-)}(x+y)$ is non-zero is shown in figure 1. Neglecting the regions in which either $\mu = 0$ or $\nu = 0$ (or both), the relevant region is the dark-grey triangle. As μ and ν are positive measures, integration over the small square gives a lower and integration over the larger square an upper bound:

$$\int_{y_-}^{y_-+\frac{\varepsilon}{2}} \nu(\mathrm{d}y) \int_{x_-}^{x_-+\frac{\varepsilon}{2}} \mu(\mathrm{d}x) \leqslant \mu * \nu(B_\varepsilon(z_-)) \leqslant \int_{y_-}^{y_-+\varepsilon} \nu(\mathrm{d}y) \int_{x_-}^{x_-+\varepsilon} \mu(\mathrm{d}x). \tag{3.9}$$

Taking into account that $\mu = 0$ on $(x_- - \varepsilon, x_-)$ and $\nu = 0$ on $(y_- - \varepsilon, y_-)$ we can write

$$\nu(B_{\frac{\varepsilon}{2}}(y_-))\mu(B_{\frac{\varepsilon}{2}}(x_-)) \leqslant \mu * \nu(B_\varepsilon(z_-)) \leqslant \nu(B_\varepsilon(y_-))\mu(B_\varepsilon(x_-)) \tag{3.10}$$

to finally obtain

$$\begin{aligned} \frac{\ln \nu(B_{\frac{\varepsilon}{2}}(y_-)) + \ln \mu(B_{\frac{\varepsilon}{2}}(x_-))}{\ln \frac{\varepsilon}{2} + \ln 2} &\geqslant \frac{\ln \mu * \nu(B_\varepsilon(z_-))}{\ln \varepsilon} \\ &\geqslant \frac{\ln \nu(B_\varepsilon(y_-)) + \ln \mu(B_\varepsilon(x_-))}{\ln \varepsilon} \end{aligned} \tag{3.11}$$

which completes the proof as both sides of the inequality converge to $D_p(x_-;\mu)+D_p(y_-;\nu)$ as $\varepsilon\to 0$. The proof for the right-hand boundaries is obtained by applying the same arguments to $\tilde{\mu}(X):=\mu(-X)$ and $\tilde{\nu}(X):=\nu(-X)$. □

To apply lemma 3.3 to the measure of the local magnetization in the one-dimensional RFIM it is important to know how the mappings $A_\#$ and $\tanh\beta_\#$ in (2.14) influence the pointwise dimensions of $\mu^{(m)}$. It turns out that they are of no significance in this context because the pointwise dimension of the image measure at the image of some point is the pointwise dimension of the original measure at this point if the map under consideration is bi-Lipschitz.

Lemma 3.4 (Stability of D_p with respect to bi-Lipschitz maps). *Let $f:\mathbb{R}\to\mathbb{R}$ be a bi-Lipschitz function and μ a bounded Borel measure on $\mathbb{R}$. Then $D_p(f(x);f_\#(\mu))=D_p(x;\mu)$.*

Proof. As f is bi-Lipschitz so is f^{-1} and therefore

$$L^{-1}|y-x|\leqslant|f^{-1}(y)-f^{-1}(x)|\leqslant L|y-x| \tag{3.12}$$

for some constant $L>1$. Then

$$|f^{-1}(f(x)+\varepsilon)-x|=|f^{-1}(f(x)+\varepsilon)-f^{-1}(f(x))|\leqslant L|f(x)+\varepsilon-f(x)|=L\varepsilon \tag{3.13}$$

and

$$|x-f^{-1}(f(x)-\varepsilon)|\leqslant L|f(x)-(f(x)-\varepsilon)|=L\varepsilon. \tag{3.14}$$

This implies $f^{-1}(B_\varepsilon(f(x)))\subseteq B_{L\varepsilon}(x)$. In the same way one obtains $B_{L^{-1}\varepsilon}(x)\subseteq f^{-1}(B_\varepsilon(f(x)))$ such that

$$\frac{\ln\mu(B_{L^{-1}\varepsilon}(x))}{\ln L^{-1}\varepsilon+\ln L}\geqslant\frac{\ln f_\#\mu(B_\varepsilon(f(x)))}{\ln\varepsilon}\geqslant\frac{\ln\mu(B_{L\varepsilon}(x))}{\ln L\varepsilon-\ln L}. \tag{3.15}$$

The left- and the right-hand side of the inequality converge to $D_p(x;\mu)$ such that the middle part which converges to $D_p(f(x);f_\#\mu)$ also converges to this limit. □

For bounded measures with compact support it is sufficient that the function f is bi-Lipschitz on an interval containing the support of the measure. As $A(\cdot)$ and $\tanh\beta(\cdot)$ are bi-Lipschitz on any finite interval lemmas 3.3 and 3.4 directly imply $D_p(m_-;\mu^{(m)})=D_p(m_-;\tanh\beta_\#(\mu^{(x)}*A_\#\mu^{(x)}))=D_p(x_-;\mu^{(x)})+D_p(A(x_-);A_\#\mu^{(x)})=2D_p(x_-;\mu^{(x)})$. In [9] lower (upper) bounds on D_q for $q<0$ ($q>0$) based on the pointwise dimension at arbitrary points in the support of the measure were developed. These bounds can directly be applied to the D_q-spectrum of $\mu^{(m)}$, resulting in

$$D_q(\mu^{(m)})\geqslant\frac{q}{q-1}2D_p(x_-)=\frac{q}{1-q}\frac{2\ln 2}{\ln A'(x_-)}\qquad(q<0). \tag{3.16}$$

This bound is a tight bound as long as the pointwise dimension at the boundary is weak. This is the case as long as $D_p(m_-)>1$. The critical value $h_c^{(m,3)}$ determined by this condition is

$$\frac{1}{2\beta}\ln\left(\frac{R+\mathrm{e}^{2\beta J}}{R^{-1}+\mathrm{e}^{2\beta J}}\right) \tag{3.17}$$

with

$$R=3\sinh(2\beta J)-\mathrm{e}^{-2\beta J}+\sqrt{\left(3\sinh(2\beta J)-\mathrm{e}^{-2\beta J}\right)^2-1}. \tag{3.18}$$

The critical value can also be interpreted in terms of the measure density. At this value of h the measure density at the boundary of the support changes from 0 (for $h<h_c^{(m,3)}$) to ∞ (for $h>h_c^{(m,3)}$).

For $q > 0$ the corresponding bound is not of interest as the smoothness of $p^{(x)}$ in the region of small h implies smoothness of $p^{(m)}$ in this region and thus $D_q = 1$ for all $q > 0$. The same applies to the connectedness of the support, implying $D_0 = 1$.

The formerly discussed [9, 11] transition in the density of the effective field in which the slope of the coarse-grained measure density at the boundary of the support changes from 0 to ∞ also has an analogue. This effect occurs for the coarse-grained measure density of the magnetization at $D_p(m_-) = \frac{1}{2}$ corresponding to

$$h_c^{(m,4)} = \frac{1}{\beta}\operatorname{arsinh}\left(2^{-\frac{3}{2}}(1 - 9\mathrm{e}^{-4\beta J})^{\frac{1}{2}}\right) = h_c^{(3)}. \tag{3.19}$$

Note that the measure density of the local magnetization changes its slope at the boundary at the same critical value at which the measure density of the effective field at the boundary changes from 0 to ∞ (cf [9, 11]).

Apart from the relation between the pointwise dimensions of the convolution and its factors discussed so far there also exists a general relation between the D_q-spectra.

Theorem 3.5 (Upper bound on $D_q(\mu * \nu)$). *The D_q-spectrum of the convolution is bounded from above by the sum of the D_q-spectra of the factors,*

$$D_q(\mu * \nu) \leqslant D_q(\mu) + D_q(\nu). \tag{3.20}$$

Proof. We need to distinguish three cases, $q > 1$, $0 < q < 1$ and $q < 0$. For the first two cases the improved multifractal formalism with enlarged boxes coincides with the usual one and for simplicity we will use the latter in these cases. Throughout the proof sums of the form $\sum_i \mu_i^q$ extend over all $i \in \mathbb{Z}$ with $\mu_i > 0$, i.e. boxes with zero measure are not taken into account (which is important for $q \leqslant 0$). Let $\varepsilon > 0$. We denote $x_i := \frac{\varepsilon}{2}i$, $i \in \mathbb{Z}$.

Let $q > 1$. For any $i \in \mathbb{Z}$

$$(\mu * \nu)_i := \mu * \nu(B_{\frac{\varepsilon}{2}}(x_{2i})) = \iint \mathbf{1}_{B_{\frac{\varepsilon}{2}}(x_{2i})}(x + y)\mu(\mathrm{d}x)\nu(\mathrm{d}y) \tag{3.21}$$

is the integral over the diagonal strip in the (x, y)-plane shown in figure 2(a). Integration over the dark-grey squares provides a lower bound on this integral.

$$(\mu * \nu)_i \geqslant \sum_j \mu(B_{\frac{\varepsilon}{4}}(x_{2i+j}))\nu(B_{\frac{\varepsilon}{4}}(x_{2i-j})). \tag{3.22}$$

Taking the qth power of both sides and using $(\sum_i x_i)^q \geqslant \sum_i x_i^q$ for $q > 1$ and any positive numbers x_i we obtain

$$(\mu * \nu)_i^q \geqslant \sum_j \mu(B_{\frac{\varepsilon}{4}}(x_{2i+j}))^q \nu(B_{\frac{\varepsilon}{4}}(x_{2i-j}))^q. \tag{3.23}$$

For $(\mu * \nu)_i'^q := \mu * \nu(B_{\frac{\varepsilon}{2}}(x_{2i+1}))^q$ we have in the same way

$$(\mu * \nu)_i'^q \geqslant \sum_j \mu(B_{\frac{\varepsilon}{4}}(x_{2i+j+1}))^q \nu(B_{\frac{\varepsilon}{4}}(x_{2i-j}))^q. \tag{3.24}$$

We denote $\mu_i := \mu(B_{\frac{\varepsilon}{4}}(x_i))$ and $\nu_j := \nu(B_{\frac{\varepsilon}{4}}(x_j))$. Summing (3.23) and (3.24) and over all i we obtain on the right-hand side $\sum_i \sum_j \mu_i \nu_j$. It is straightforward to show that $\sum_i (\mu * \nu)_i'^q \leqslant 2^{q+1} \sum_i (\mu * \nu)_i^q$ (cf appendix) such that the left-hand side of the sum of (3.23) and (3.24) summed over all i is less than or equal to $(2^{q+1}+1) \sum_i (\mu * \nu)_i^q$. Taking the logarithm, dividing by $\ln \varepsilon$ and multiplying by $1/(q-1)$ we obtain

$$\frac{1}{q-1}\frac{\ln \sum_i (\mu * \nu)_i^q + \ln 2^{q+1}}{\ln \varepsilon} \leqslant \frac{1}{q-1}\frac{\ln \sum_i \mu_i^q + \ln \sum_j \nu_j^q}{\ln \frac{\varepsilon}{2} + \ln 2} \tag{3.25}$$

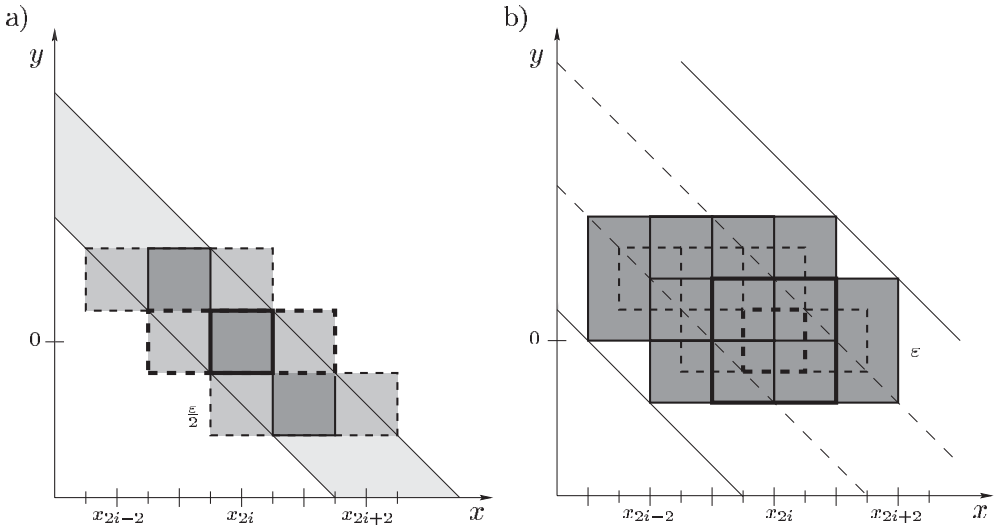

Figure 2. Illustration of the main ideas of the proof of theorem 3.5. Figure (*a*) applies to $q > 0$ and figure (*b*) to $q < 0$. The diagonal strip in (*a*) represents the region of integration for $(\mu * \nu)_i$, the measure of one of the disjoint intervals of length ε covering supp $\mu * \nu$. The integral over the dark grey squares (and diagonally translated disjoint copies) provides a lower bound on $(\mu * \nu)_i$ used in the case $q > 1$. Considering additionally the integral over the dashed squares gives an upper bound on $(\mu * \nu)_i$ needed in the case $0 < q < 1$. The wide diagonal strip in (*b*) is the region of integration for $(\mu * \nu)_i$, the measure of one of the (intersecting) enlarged intervals of length 3ε covering supp $\mu * \nu$. The narrow dashed strip is the region of integration for the corresponding inner interval of size ε. Integration over each of the six overlapping large squares of side length ε (solid lines) and their disjoint by $(-n\varepsilon, n\varepsilon)$ diagonally translated copies gives a lower bound on $(\mu * \nu)_i$ such that the sum of the six integrals gives a lower bound on $6(\mu * \nu)_i$. The narrow strip is contained in the union of all the interior small squares of side length $\frac{\varepsilon}{2}$ (dashed lines), assuring that the lower bound obtained is non-zero whenever the integral over the narrow strip is. This is an important point in the proof. The details are given in the text.

which completes the proof for $q > 1$ as the left-hand side converges to $D_q(\mu * \nu)$ and the right-hand side to $D_q(\mu) + D_q(\nu)$ as $\varepsilon \to 0$.

Let $0 < q < 1$ and $i \in \mathbb{Z}$. We again write $(\mu * \nu)_i := \mu * \nu(B_{\frac{\varepsilon}{2}}(x_{2i}))$, $\mu_i := \mu(B_{\frac{\varepsilon}{4}}(x_i))$ and $\nu_j := \nu(B_{\frac{\varepsilon}{4}}(x_j))$. The solid and dashed squares in figure 2(*a*) and by $(n\varepsilon, -n\varepsilon)$ diagonally translated disjoint copies cover the diagonal strip over which we need to integrate to obtain $(\mu * \nu)_i$. We therefore have the upper bound

$$(\mu * \nu)_i \leqslant \sum_j \sum_{k=-1}^{1} \mu_{2i+j+k} \nu_{2i-j}. \tag{3.26}$$

Taking the qth power and using $(\sum_i x_i)^q \leqslant \sum_i x_i^q$ for $q < 1$ and arbitrary positive numbers x_i yields

$$(\mu * \nu)_i^q \leqslant \sum_j \sum_{k=-1}^{1} \mu_{2i+j+k}^q \nu_{2i-j}^q. \tag{3.27}$$

When summing over all i each combination $\mu_i \nu_j$ appears at most twice in the sum on the right-hand side such that

$$\sum_i (\mu * \nu)_i^q \leqslant 2 \sum_i \sum_j \mu_i^q \nu_j^q. \tag{3.28}$$

Taking the logarithm of both sides, dividing by $\ln \varepsilon$ and multiplying with $1/(q-1)$ results in

$$\frac{1}{q-1}\frac{\ln \sum_i (\mu * \nu)_i^q}{\ln \varepsilon} \leqslant \frac{1}{q-1}\frac{\ln \sum_i \mu_i^q + \ln \sum_j \nu_j^q + \ln 2}{\ln \frac{\varepsilon}{2} + \ln 2}. \tag{3.29}$$

The limit $\varepsilon \to 0$ yields $D_q(\mu * \nu) \leqslant D_q(\mu) + D_q(\nu)$.

Let $q < 0$. In this case we need the improved multifractal formalism with enlarged intervals. We use the notation

$$(\mu * \nu)_i := \begin{cases} \mu(B_{\frac{3}{2}\varepsilon}(x_{2i})) & (\mu * \nu(B_{\frac{\varepsilon}{2}}(x_{2i})) > 0) \\ 0 & (\text{otherwise}). \end{cases} \tag{3.30}$$

By this choice we enlarge the ε-intervals by ε on both sides corresponding to $\kappa = 1$ in Riedi's notation [40]. Furthermore we denote

$$\mu_i := \begin{cases} \mu(B_{\frac{\varepsilon}{2}}(x_i)) & (\mu(B_{\frac{\varepsilon}{4}}(x_i)) \geqslant 0) \\ 0 & (\text{otherwise}) \end{cases} \qquad \nu_i := \begin{cases} \nu(B_{\frac{\varepsilon}{2}}(x_i)) & (\nu(B_{\frac{\varepsilon}{4}}(x_i)) \geqslant 0) \\ 0 & (\text{otherwise}) \end{cases} \tag{3.31}$$

i.e. the $\frac{\varepsilon}{2}$-intervals of μ and ν are enlarged by $\frac{\varepsilon}{4}$, corresponding to $\kappa = \frac{1}{2}$. This choice facilitates the proof and has no influence on the resulting D_q as Riedi has shown (cf [40]). Let $i \in \mathbb{Z}$ with $(\mu * \nu)_i > 0$, i.e. the integral over the ith interior interval is non-zero. When calculating $(\mu * \nu)_i$ we integrate over the wide diagonal strip in figure 2(b). The large squares $B_{\frac{\varepsilon}{2}}(x_{2i+2j}) \times B_{\frac{\varepsilon}{2}}(x_{2i-2j})$, $j \in \mathbb{Z}$, are disjoint and are all contained in the strip. Therefore,

$$(\mu * \nu)_i \geqslant \sum_j \mu_{2i+2j}\nu_{2i-2j}. \tag{3.32}$$

This applies analogously to the other five squares shown and their disjoint copies diagonally translated by $(n\varepsilon, -n\varepsilon)$ such that

$$6(\mu * \nu)_i \geqslant \sum_j \sum_{k=-1}^{1} \mu_{2i+j+k}\nu_{2i-j}. \tag{3.33}$$

The integral over the narrow diagonal strip determines that $(\mu * \nu)_i$ is greater than zero. In the same way the integral over the small squares determines whether the terms on the right-hand side are greater than zero. As the narrow strip is contained in the union of the small squares, the right-hand side is greater than zero as $(\mu * \nu)_i$ is. We therefore can take the qth power on both sides and (omitting all zero terms) use $(\sum_i x_i)^q \leqslant \sum_i x_i^q$ for $q < 1$ and arbitrary positive numbers x_i to obtain

$$6^q(\mu * \nu)_i^q \leqslant \sum_j \sum_{k=-1}^{1} \mu_{2i+j+k}^q \nu_{2i-j}^q. \tag{3.34}$$

When summing over all i with $(\mu * \nu)_i > 0$, each combination $\mu_i^q \nu_j^q$ appears at most twice. Furthermore, adding terms which do not already appear only enlarges the right-hand side. Therefore,

$$6^q \sum_i (\mu * \nu)_i^q \leqslant 2 \sum_i \mu_i^q \sum_j \nu_j^q. \tag{3.35}$$

From this we immediately obtain

$$\frac{1}{q-1}\frac{\ln \sum_i (\mu * \nu)_i^q + \ln 6^q}{\ln \varepsilon} \leqslant \frac{1}{q-1}\frac{\ln \sum_i \mu_i^q + \ln \sum_j \nu_j^q + \ln 2}{\ln \frac{\varepsilon}{2} + \ln 2} \tag{3.36}$$

which implies $D_q(\mu * \nu) \leqslant D_q(\mu) + D_q(\nu)$ in the limit $\varepsilon \to 0$. □

Note that this proof easily generalizes to measures on $\mathbb{R}^n$. In [40] the invariance of the D_q-spectrum with respect to bi-Lipschitz maps was shown, i.e. if $f : \mathbb{R} \to \mathbb{R}$ is a bi-Lipschitz map then

$$D_q(\mu) = D_q(f_\#(\mu)). \tag{3.37}$$

As in the case of the pointwise dimension it is sufficient that the function f is bi-Lipschitz on an interval containing the support of μ. Therefore, we can immediately deduce from theorem 3.5 and (3.37) that

$$\begin{aligned} D_q(\mu^{(m)}) &= D_q(\mu^{(x)} * A_\#\mu^{(x)}) \\ &\leqslant D_q(\mu^{(x)}) + D_q(A_\#\mu^{(x)}) = 2D_q(\mu^{(x)}). \end{aligned} \tag{3.38}$$

As the D_q-spectrum of the invariant measure of the effective field is—at least on a numerical level—very well known (cf [9]), this provides interesting insights for the D_q-spectrum of the measure of the local magnetization (cf figure 7). In section 5 we will discuss how to obtain the D_q-spectrum of the measure of the local magnetization numerically and we will compare the results with the bounds obtained in this section.

4. Convolution of measures on Cantor sets

Let $\mathcal{C}_a^{(0)} = [-\frac{1}{2}, \frac{1}{2}]$ and $\mathcal{C}_a^{(n)}$ be defined inductively by $\mathcal{C}_a^{(n)} := f_{a+}(\mathcal{C}_a^{(n-1)}) \cup f_{a-}(\mathcal{C}_a^{(n-1)})$ with $f_{a+}(x) = ax + \frac{1-a}{2}$ and $f_{a-} = ax - \frac{1-a}{2}$. The infinite intersection $\mathcal{C}_a := \bigcap_{n=0}^{\infty} \mathcal{C}_a^{(n)}$ is the a-Cantor set. On the approximating sets $\mathcal{C}_a^{(n)}$ we define the probability densities

$$p_{a,p}^{(n)}(x) = \frac{p}{a} p_{a,p}^{(n-1)}(f_{a+}^{-1}(x)) + \frac{1-p}{a} p_{a,p}^{(n-1)}(f_{a-}^{-1}(x)). \tag{4.1}$$

The corresponding measures are denoted by $\mu_{a,p}^{(n)}(X) = \int_X p_{a,p}^{(n)} \,\mathrm{d}x$ for any $X \in \mathcal{B}(\mathbb{R})$. The measures $\mu_{a,p}^{(n)}$ converge to a limit measure $\mu_{a,p}$, which is often referred to as an a-Cantor set with weights p and $1-p$. For a generic choice of a and p the measure $\mu_{a,p}$ is a multifractal. For an illustration cf figures 3 and 4. In the following example we calculate the D_q-spectrum of the convolution of $\mu_{a,p}$ with $\lambda_\#\mu_{a,p}$, a 'compressed' version of itself ($\lambda \leqslant 1$). As this is in general a hard problem we discuss two examples.

Example 4.1. Let $0 < p < 1$ and $a/(1-2a) \leqslant \lambda \leqslant (1-2a)$. This is meaningful for $a \leqslant \frac{1}{4}$. Then, the two intervals of supp $\mu_{a,p}^{(1)}$ fit into the gap of supp $\lambda_\#\mu_{a,p}^{(1)}$ and on the other hand the complete supp $\lambda_\#\mu_{a,p}^{(1)}$ fits into the gap of supp $\mu_{a,p}^{(1)}$. Self-similarity of $\mathcal{C}_a$ and $\lambda_\#\mathcal{C}_a$ imply that for any given n and $y \in \mathbb{R}$ at most one pair of bars in $p_{a,p}^{(n)}(x)$ and $\lambda_\# p_{a,p}^{(n)}(y-x)$ can overlap. The convolution is therefore a collection of trapezoids as shown in figure 3. We denote the intervals of supp $\mu_{a,p}^{(n)} * \lambda_\#\mu_{a,p}^{(n)}$ (the bases of the trapezoids) by $T_j^{(n)}$, $j = 1, \ldots, 2^n$. For larger n only the structure of the measure within the trapezoids but not their total measure changes, i.e. $\mu_{a,p} * \lambda_\#\mu_{a,p}(T_j^{(n)}) = \mu_{a,p}^{(n)} * \lambda_\#\mu_{a,p}^{(n)}(T_j^{(n)})$. We can therefore use $\mu_{a,p} * \lambda_\#\mu_{a,p}$ and $\mu_{a,p}^{(n)} * \lambda_\#\mu_{a,p}^{(n)}$ interchangeably. This fortunate circumstance is due to the fact that the self-similarity of the Cantor sets induces a direct iteration for the convolution, making it self-similar itself. The analytical treatment of the D_q-spectrum in this example is essentially based on this fact. If we choose $\varepsilon_n := a^n + \lambda a^n$, which is the width of the trapezoids at level n, boxes $B_{\frac{3}{2}\varepsilon_n}(x_i)$, $x_i = i\varepsilon_n$, $i \in \mathbb{Z}$ with $\mu_{a,p}(B_{\frac{\varepsilon_n}{2}}(x_i)) > 0$ contain at least one whole trapezoid of level n and intersect at most four. Thus, denoting

$$\mu_i := \begin{cases} \mu_{a,p} * \lambda_\#\mu_{a,p}(B_{\frac{3}{2}\varepsilon_n}(x_i)) & (\mu_{a,p} * \lambda_\#\mu_{a,p}(B_{\frac{\varepsilon_n}{2}}(x_i)) > 0) \\ 0 & (\text{otherwise}) \end{cases} \tag{4.2}$$

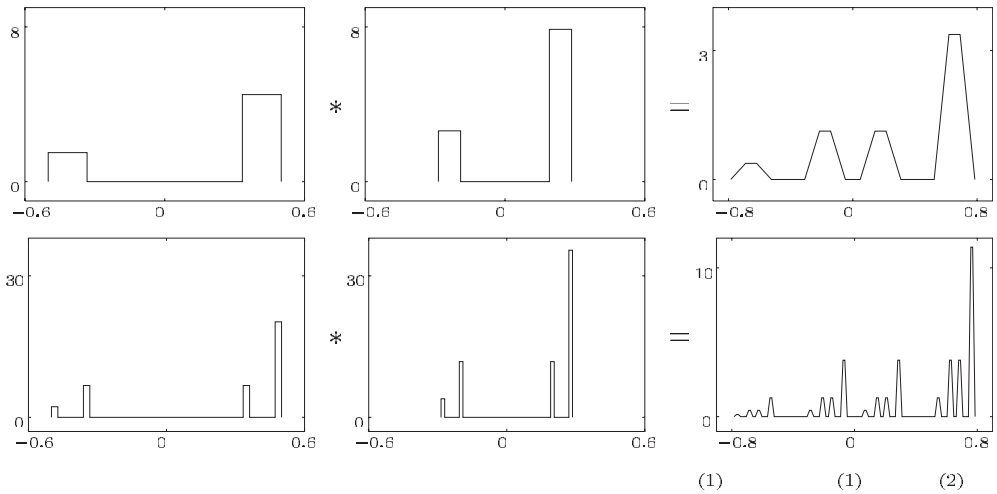

Figure 3. Illustration of the convolution of $\mu_{a,p}^{(1)}$ with $\lambda_{\#}\mu_{a,p}^{(1)}$ and $\mu_{a,p}^{(2)}$ with $\lambda_{\#}\mu_{a,p}^{(2)}$ for $a = \frac{1}{6}$, $p = \frac{3}{4}$ and $\lambda = \frac{4}{7}$. The condition for the disjointness of the trapezoids, $a/(1-2a) \leqslant \lambda \leqslant (1-2a)$, is clearly fulfilled for this choice of parameters such that in the limit $n \to \infty$ example 4.1 applies.

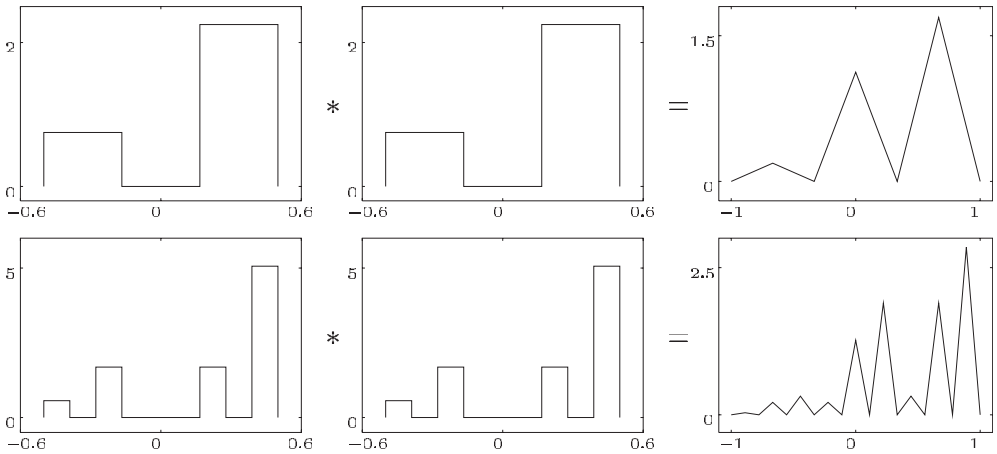

Figure 4. Illustration of the convolution of $\mu_{a,p}^{(1)}$ with itself and $\mu_{a,p}^{(2)}$ with itself for $a = \frac{1}{3}$ and $p = \frac{3}{4}$. For this choice of parameters example 4.2 applies in the limit $n \to \infty$.

we obtain for $q > 0, q \neq 1$

$$\mu_{a,p} * \lambda_{\#}\mu_{a,p}\left(T_{j(i)}^{(n)}\right)^q \leqslant \mu_i^q \leqslant \left(4 \max_{j \in J(i)} \mu_{a,p} * \lambda_{\#}\mu_{a,p}(T_j^{(n)})\right)^q \tag{4.3}$$

where $j(i)$ is the index of a trapezoid completely contained in $B_{\frac{3}{2}\varepsilon_n}(x_i)$ and $J(i)$ is the set of the indices of all trapezoids intersecting $B_{\frac{3}{2}\varepsilon_n}(x_i)$. As any trapezoid can appear at most four times on the right-hand side when summing over i and any trapezoid appears at least once on the left-hand side this implies

$$\sum_j \mu_{a,p} * \lambda_{\#}\mu_{a,p}\left(T_j^{(n)}\right)^q \leqslant \sum_i \mu_i^q \leqslant 4 \sum_j \left(4\mu_{a,p} * \lambda_{\#}\mu_{a,p}(T_j^{(n)})\right)^q. \tag{4.4}$$

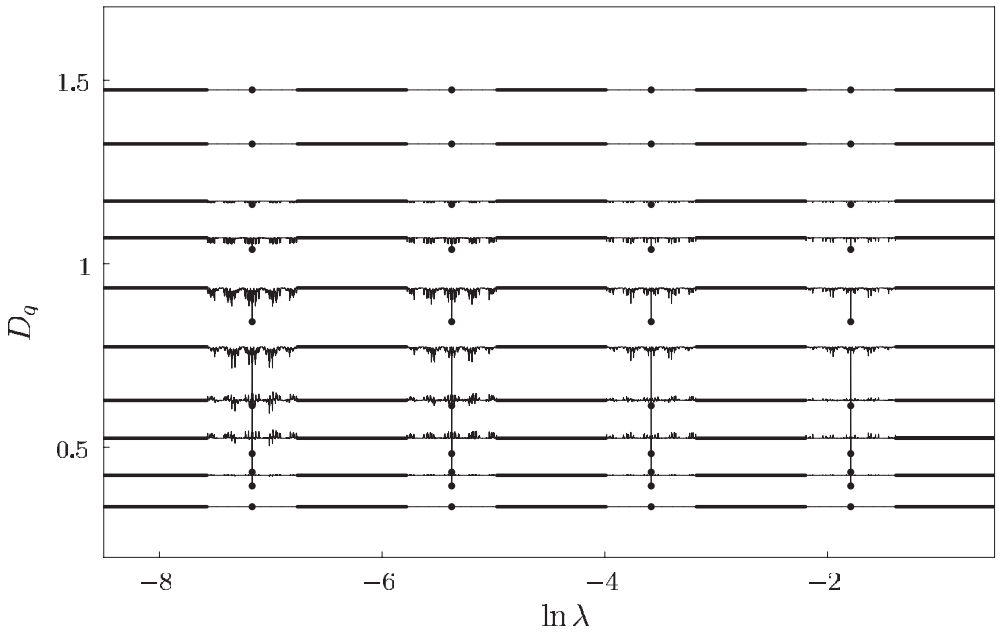

Figure 5. D_q-spectrum of $\mu_{a,p} * \lambda_\# \mu_{a,p}$ as a function of $\ln\lambda$ for $q = -20, -6, -3, -2, -1, 0, 1, 2, 4$ and 20. The thick curves are the exact D_q obtained in example 4.1 and the points the D_q obtained in example 4.2. The thin curves are numerical results obtained from iteration depths $l = r = 8$ compared to $l = r = 7$ in the new natural partition method (cf section 5.3).

The measures of the trapezoids can explicitly be calculated such that

$$\sum_j \mu_{a,p} * \lambda_\# \mu_{a,p}(T_j^{(n)})^q = \sum_{k,l=0}^{n} \binom{n}{k}\binom{n}{l}(p^k(1-p)^{n-k}p^l(1-p)^{n-l})^q. \tag{4.5}$$

Applying $\sum_k \binom{n}{k}(p^q)^k((1-p)^q)^{n-k} = (p^q + (1-p)^q)^n$ we obtain

$$(p^q + (1-p)^q)^{2n} \leqslant \sum_i \mu_i^q \leqslant 4^{q+1}(p^q + (1-p)^q)^{2n} \tag{4.6}$$

and therefore

$$D_q(\mu_{a,p}) = \frac{1}{q-1}\frac{2\ln(p^q + (1-p)^q)}{\ln a}. \tag{4.7}$$

For $q < 0$ the argument is the same with reversed inequality signs, which leads to the same result.

For $q = 1$ we calculate the limit $q \to 1$ of (4.7), yielding

$$\begin{aligned} D_1 &= \lim_{q\to 1}\frac{1}{q-1}\frac{2\ln(p^q + (1-p)^q)}{\ln a} \\ &= 2(p\ln p + (1-p)\ln(1-p))/\ln a. \end{aligned} \tag{4.8}$$

For any $\lambda \in [a^{k+1}/(1-2a), a^k(1-2a)]$, $k \in \mathbb{N}$, the arguments above apply to $\mu_{a,p}^{(n+k)} * \lambda_\# \mu_{a,p}^{(n)}$, which according to lemma 3.1 also converges to $\mu_{a,p} * \lambda_\# \mu_{a,p}$. Therefore, (4.7) and (4.8) apply to all λ taken from these intervals. (For an example cf figure 5.)

Example 4.2. Let $0 < p < 1$, $a \leqslant \frac{1}{3}$ and $\lambda = 1$. We then choose $\varepsilon_n := 2a^n$ and boxes of length ε_n in such a way that each box covers one of the spikes of $\mu_{a,p}^{(n)} * \mu_{a,p}^{(n)}$. This is a permitted choice and avoids any complications with $q < 0$ such that we refrain from using enlarged boxes here. The situation is like that shown in figure 4, i.e. for $n = 1$, $(\mu_{a,p}^{(1)} * \mu_{a,p}^{(1)})_i = (1-p)^2$, $2p(1-p)$ and p^2 for $i = 1, 2$ and 3 respectively. As in example 4.1 self-similarity implies for our specific choice of boxes that we can use $\mu_{a,p}^{(n)} * \mu_{a,p}^{(n)}$ and $\mu_{a,p} * \mu_{a,p}$ interchangeably as they coincide on all boxes. Furthermore, the result of the convolution of the next iteration, $n = 2$, can be constructed by replacing each triangle in figure 4 by the complete figure and choosing the corresponding weight. Therefore, the $(\mu_{a,p}^{(2)} * \mu_{a,p}^{(2)})_i$, $i = 1, \ldots, 9$, sum up to

$$\sum_{k=0}^{2}\sum_{l=0}^{2-k}\binom{2}{k}\binom{2-k}{l}(1-p)^{2k}(2p(1-p))^{2-k}p^{2(2-k-l)} \tag{4.9}$$

$$= \left((1-p)^2 + 2p(1-p) + p^2\right)^2. \tag{4.10}$$

This continues for larger n such that we have

$$\sum_i (\mu_{a,p}^{(n)} * \mu_{a,p}^{(n)})_i^q = \sum_{k=0}^{n}\sum_{l=0}^{n-k}\binom{n}{k}\binom{n-k}{l}\left((1-p)^{2k}(2p(1-p))^{n-k}p^{2(n-k-l)}\right)^q \tag{4.11}$$

$$= ((1-p)^{2q} + 2^q p^q (1-p)^q + p^{2q})^n. \tag{4.12}$$

For $q \neq 1$ this yields

$$D_q = \frac{1}{q-1}\lim_{n\to\infty}\frac{n\ln((1-p)^{2q} + 2^q p^q (1-p)^q + p^{2q})}{n\ln a + \ln 2} \tag{4.13}$$

$$= \frac{1}{q-1}\frac{\ln((1-p)^{2q} + 2^q p^q (1-p)^q + p^{2q})}{\ln a}. \tag{4.14}$$

The limit $q \to 1$ results in

$$D_1 = \lim_{q\to 1}\frac{1}{q-1}\frac{\ln((1-p)^{2q} + 2^q p^q (1-p)^q + p^{2q})}{\ln a}$$

$$= 2(p\ln p + p(1-p)\ln 2 + (1-p)\ln(1-p))/\ln a. \tag{4.15}$$

As in example 4.1 the arguments can be repeated for the a^n-fold value of λ such that (4.14) and (4.15) are also correct for all $\lambda = a^n$, $n \in \mathbb{N}$. This means that we can calculate the D_q-spectrum at specific points between the intervals where it is given by (4.7) and (4.8). The results are illustrated for $a = \frac{1}{6}$ and $p = \frac{3}{4}$ in figure 5.

In the case of the random-field Ising model we are interested in the dependence of the D_q-spectrum on the strength h of the random field, which rather corresponds to varying a in the convolution of Cantor sets. Viewing (4.7) and (4.8) in this light we can choose $\lambda = \frac{1}{2}$ such that for all $a < \frac{1}{4}$ example 4.1 applies. This results in the right-hand part of the D_q-spectrum shown in figure 6. For the left-hand part with a close to unity we have the usual lower bounds for $q < 0$ based on the pointwise dimension at the boundary of the support and $D_q = 1$ for $q \geqslant 1$ from the regularity of $\mu_{a,p}$.

The convolution of two-scale Cantor sets shows a far richer behaviour than the two examples above. It turns out that the lacking strict self-similarity does not allow the kind of analytical treatment we have used so far. Numerical investigations show that the D_q-spectrum strongly depends on the two scales of the Cantor sets. Furthermore, in a large parameter regime the obtained numerical estimates are extremely sensitive to the iteration depth to which the Cantor sets are generated. The situation is of similar complexity as for the measure of the local magnetization in the one-dimensional random-field Ising model discussed below. We

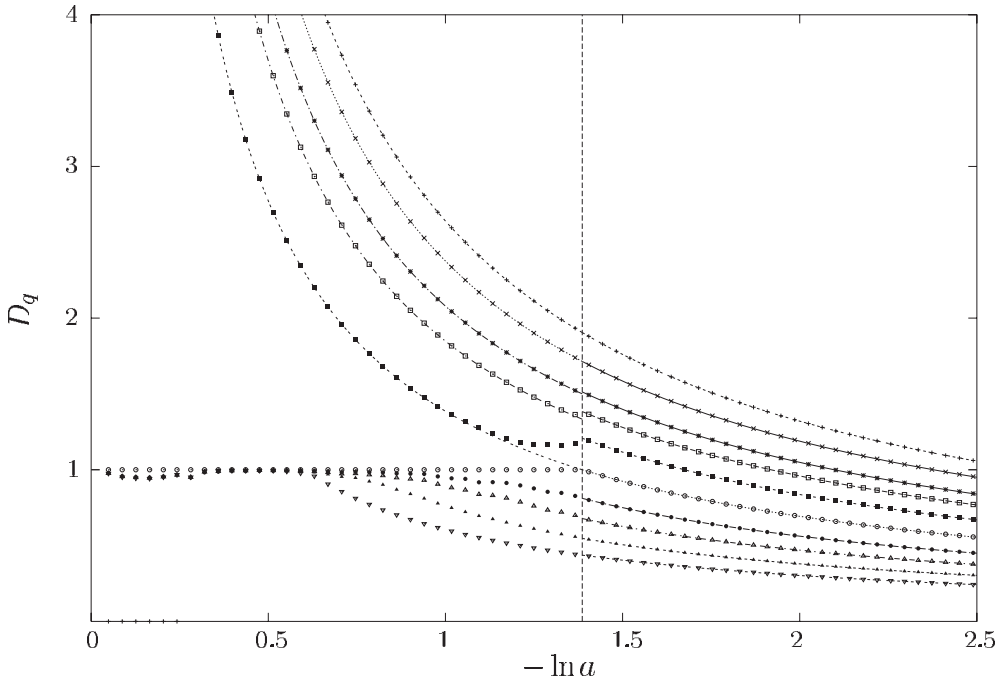

Figure 6. D_q-spectrum of $\mu_{a,p} * \lambda_\# \mu_{a,p}$ as a function of $-\ln a$ with $p = \frac{3}{4}$, $\lambda = \frac{1}{2}$ and $q = -20$, -6, -3, -2, -1, 0, 1, 2, 4 and 20. The curves to the left of $-\ln a = \ln 4$ are the usual lower bounds based on the pointwise dimension at the left-hand boundary of $\mathcal{C}_{a,p}$. The curves on the right are the calculated exact values of D_q according to (4.7) and (4.8). The points are numerical results for iteration depths $l = r = 6$ compared with $l = r = 5$.

therefore refrain from discussing this case and turn to the characterization of the measure of the local magnetization.

5. D_q-spectrum of the local magnetization

In this section we present our numerical methods and the resulting D_q-spectra for the measure of the local magnetization in the random-field Ising model. We obtain the D_q-spectrum of the measure of the local magnetization in several steps.

5.1. Generation of the measure of the effective field

The measure of the local magnetization in the bulk of the random-field Ising chain is given by (2.11), i.e. it is the convolution of the measure of the effective field x_n with a distorted version of itself. Therefore, as a first step for a numerical treatment, an approximation of this measure is needed. It turns out that a very useful approximation is the following (cf [9, 11]). We take the partition of the invariant interval $I = [x_-^*, x_+^*]$ given by the points $\{x_i\} = \{f_{\{\sigma\}_n}(x_-^*), f_{\{\sigma\}_n}(x_+^*)\}$. It is sometimes called the 'new natural partition' (cf [11]). The points x_-^* and x_+^* are the fixed points of the iteration (2.4). The symbols $f_{\{\sigma\}_n}(x)$ denote the iterated functions $f_{\{\sigma\}_n}(x) := f_{\sigma_1} \circ f_{\sigma_2} \circ \cdots \circ f_{\sigma_n}(x)$ with $f_+(x) = A(x)+h$, $f_-(x) = A(x)-h$ and $\{\sigma\} = \{\sigma_1, \sigma_2, \ldots, \sigma_n\}$ with $\sigma_i \in \{+, -\}$. The n-fold application of the Frobenius–Perron

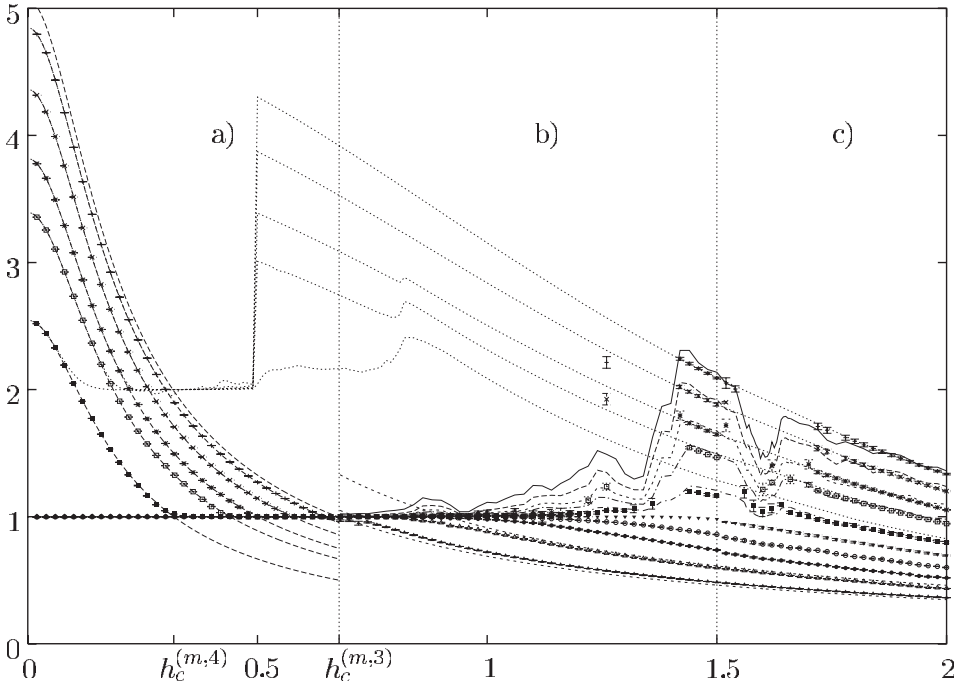

Figure 7. Numerical results for the D_q-spectrum of the measure of the local magnetization in the bulk. We considered $q = -20, -6, -3, -2, -1, 0, 1, 2, 4$ and 20. All points with error bars were obtained by the method based on the new natural partition. In regions (a) and (b) and $q \neq 0$ the results of all combinations of iteration depths $l = r = 8$, $l = r = 9$ and $l = r = 10$ were used and the number representation was C++ long doubles. In region (c) and also $q \neq 0$ all combinations of iteration depths $l = r = 5$, $l = r = 6$ and $l = r = 7$ were used with numbers of the arbitrary precision library 'CLN' with guaranteed 50 decimal digits. The error bars are obtained from the standard deviations of the average of the results of the three possible combinations of iteration depths. All points with standard deviation greater than 0.05 are not shown. For $q = 0$ we used iteration depths up to $l = r = 13$. The dashed curves in (a) are lower bounds on D_q and the dashed curves in (b) and (c) are upper bounds both based on the pointwise dimension at the boundary of the support of $\mu^{(m)}$. The dotted curves are the twofold numerical results for the D_q ($q < 0$) of the effective field (cf [9]) and are thus upper bounds on the D_q ($q < 0$). Finally, the other curves in (b) and (c) are the results for D_q ($q < 0$) obtained by the box scaling approach. The usual spacing in h for all data points is 0.02 except for the region between $h = 0.56$ and $h = 0.66$, where we chose a finer spacing of $\Delta h = 0.005$ in the box method. $\beta = J = 1$.

equation (2.7) on some initial distribution P_0 yields [11]

$$P_n(x) = \frac{1}{2^n} \sum_{\{\sigma\}_n} P_0(f^{-1}_{\{\sigma\}_n}(x)) \tag{5.1}$$

where the sum is taken over all symbolic sequences $\{\sigma\}_n$ for which $f^{-1}_{\{\sigma\}_n}(x)$ exists. In the numerical treatment we start with an equipartition on I,

$$P_0 = \begin{cases} 0 & (x < x^*_-) \\ (x - x^*_-)/|I| & (x \in I) \\ 1 & (x > x^*_+). \end{cases} \tag{5.2}$$

We then calculate the measure $\mu^{(x)}_n([x_i, x_{i+1}]) = P_n(x_{i+1}) - P_n(x_i)$ on the intervals of the new natural partition and approximate the density $p^{(x)}_n$ as constant within these intervals. The resulting histogram $\tilde{p}^{(x)}_n$ is used for the convolution.

5.2. Convolution

The next step toward the D_q-spectrum of the measure of the local magnetization is to calculate the convolution (2.14). We will need to calculate the measure of some given intervals, say $[m_i, m_{i+1}]$. It is given by

$$\begin{aligned}\mu_{l,r}^{(m)}([m_i, m_{i+1}]) &= \tanh\beta_{\#}(\mu_l^{(x)} * A_{\#}\mu_r^{(x)})([m_i, m_{i+1}]) \\ &= \int_{1/\beta\tanh^{-1}(m_i)}^{1/\beta\tanh^{-1}(m_{i+1})} \mathrm{d}y\, p_r^{(x)}(y) \int \mathrm{d}x\, p_l^{(x)}(x - A(y)). \end{aligned} \tag{5.3}$$

For $p_r^{(x)}$ and $p_l^{(x)}$ we substitute our piecewise constant approximations $\tilde{p}_r^{(x)}$ and $\tilde{p}_l^{(x)}$ and denote the inner integral as $F(y)$. This function is piecewise of the form $\kappa_i A(y) + \eta_i$ and thus can be represented by the coefficients κ_i, η_i and the endpoints y_i of the intervals $[y_i, y_{i+1}]$ on which the particular κ_i and η_i are valid. The outer integral in (5.3) is therefore approximately

$$\sum_i \int_{y_i}^{y_{i+1}} \tilde{p}_r^{(x)}(y)(\kappa_i A(y) + \eta_i)\,\mathrm{d}y. \tag{5.4}$$

As $\tilde{p}_r^{(x)}$ is piecewise constant this integral can easily be calculated provided $\int A(y)\,\mathrm{d}y$ is known. This integral is given by

$$\int^x A(y)\,\mathrm{d}y = \frac{1}{4\beta^2}(\mathrm{Li}_2(-\mathrm{e}^{2\beta(x-J)}) - \mathrm{Li}_2(-\mathrm{e}^{2\beta(x+J)})) - Jx + C \tag{5.5}$$

in which Li_2 denotes the second polylogarithmic function[1].

It turns out however that for the short intervals we need to integrate on the implementation of the polylogarithmic function Li_2 for double-precision numbers is less precise than a simple fifth-order Taylor expansion of $\int A(y)\,\mathrm{d}y$ around the centre of the intervals $[y_i, y_{i+1}]$. We therefore use the expansion in our numerical studies.

By the methods described thus far we have gained the ability to obtain the measure $\mu_{l,r}^{(m)}$ of any given interval $[m_i, m_{i+1}]$ and not too large iteration depths l and r. We now use two different methods to estimate the D_q-spectrum of $\mu^{(m)}$ based on this.

5.3. Determination of the D_q-spectrum

The first method uses coverings of supp $\mu_{l,r}^{(m)}$ with boxes of equal size. We choose boxes of size $\varepsilon_k := \varepsilon_0 \cdot s^k$, $k = 1, 2, \ldots, N$, for some $s < 1$ and points $x_i = i\varepsilon_k$, $i \in \mathbb{Z}$. We then calculate

$$Z_k^{(B)} = \sum_{(i)} (\mu_{l,r}^{(m)}(B_{\frac{3}{2}\varepsilon_k}(x_i)))^q \tag{5.6}$$

in which only indices i fulfilling $\mu_{l,r}^{(m)}(B_{\frac{\varepsilon_k}{2}}(x_i)) > 0$ are considered. A linear fit of $\ln Z_k^{(B)}$ as a function of $\ln\varepsilon_k$ yields $\ln Z_k^{(B)} \sim \tau_q \ln\varepsilon_k + \text{const}$ providing the desired estimate $D_q = \tau_q/(q-1)$ of the generalized fractal dimension D_q.

The second method is based on the stationarity of a suitably chosen partition function. When observing the process of the convolution of $\mu_l^{(x)}$ and $A_{\#}\mu_r^{(x)}$ more closely it becomes clear that there is a qualitative change whenever bands of $\mu_l^{(x)}$ and bands of $A_{\#}\mu_r^{(x)}$ start or cease to overlap, i.e. for values m_i of the magnetization obeying the condition

$$\frac{1}{\beta}\mathrm{artanh}(m_i) - g(x_{l,j}) = x_{r,k} \tag{5.7}$$

[1] The second polylogarithmic function is $\mathrm{Li}_2(z) := \sum_{k=1}^{\infty} \frac{z^k}{k^2} = -\int_0^z \frac{\log(1-t)}{t}\,\mathrm{d}t$.

where $x_{l,j}$ and $x_{r,k}$ are points of the new natural partition of $\mu_l^{(x)}$ and $\mu_r^{(x)}$ respectively. This condition leads to

$$m_i = \tanh\beta(f_{\{\sigma\}_l}(x_\pm^*) + A(f_{\{\tilde{\sigma}\}_r}(x_\pm^*))). \tag{5.8}$$

We will employ these points as a new natural partition for the measure of the local magnetization. It turns out that there exists a natural degeneracy within the set $\{m_i\}$ induced by the trivial identity

$$A(a) + f_-(b) = A(b) + f_-(a) \tag{5.9}$$

and other such identities comprising higher iterations of f_+ and f_-. These degeneracies have to be removed 'by hand' by the algorithm. In the spirit of [42] we then define the partition function

$$Z_{l,r}(q,\tau_q) = \sum_i \frac{\mu_{l,r}^{(m)}([m_{i+1}, m_i])^q}{(m_{i+1} - m_i)^{\tau_q}} \tag{5.10}$$

on this new natural partition and determine D_q from the condition

$$\ln Z_{l,r}(q,\tau_q) - \ln Z_{l',r'}(q,\tau_q) \stackrel{!}{=} 0 \tag{5.11}$$

with some iteration depths l, r, l', r'.

Figure 7 shows a summary of the obtained numerical results. In region (a) the behaviour of the D_q with negative q is dominated by the pointwise dimension at the boundary of the support of $\mu^{(m)}$ such that the lower bounds based on it coincide with the obtained numerical values. Furthermore, the numerical results are very stable for all iteration depths. We do not show the result of the box method in this region as it is known that box methods systematically underestimate D_q for $q < 0$ if it strongly depends on only few points in the support. The generalized dimensions for $q > 0$ are all unity because the measure is smooth. The numerical results are in perfect agreement with this statement.

In region (b) all D_q for $q < 0$ are unity for $h \gtrsim h_c^{(m,3)}$. At some point they again are greater than unity. In this region the method based on the new natural partition yields completely different results for different iteration depths. We therefore are not able to deduce the asymptotic behaviour from the scaling in finite iteration depth. Most data points had to be left out for this reason. Provided h is large enough ($h \gtrsim 1.7$) the numerical results of the new natural partition method are again stable for all iteration depths, which leads to small error bars in figure 7. For $q > 0$ we have in regions (b) and (c) perfect agreement with the upper bounds obtained from the pointwise dimension at the boundary of the support of $\mu^{(m)}$.

The difficulties in obtaining the asymptotic scaling for $q < 0$ in the region $1 \lesssim h \lesssim 1.7$ are of the same type as encountered in the convolution of two-scale Cantor sets. This shows that this is an effect of more than one relevant scale present (infinitely many in this case). As the asymptotic scaling seems not to be attainable we have the impression that from a physicist's point of view we should pose the question of what an experimentalist would observe. In any experiment the scale of resolution is bounded from below. This corresponds to the situation of the box method where the scale is bounded by the size of the smallest box (whereas the scale in the new natural partition can become more or less arbitrarily small even for finite iteration depths). We therefore surmise that the D_q-estimates based on the box method are the physical results in this region. As it turns out the results of the box method are fairly robust against changes in the iteration depth whereas they depend on an appropriate choice of box sizes. As a rule of thumb the smallest box size should be of the order of the length of the longest band of the new natural partition. The results of the box method are shown as curves in regions (b) and (c) in figure 7.

The local minimum of the D_q, $q < 0$, at $h \approx 1.6$ can be understood as a change in the overlap structure of bands of the new natural partition of the two convoluted measures for

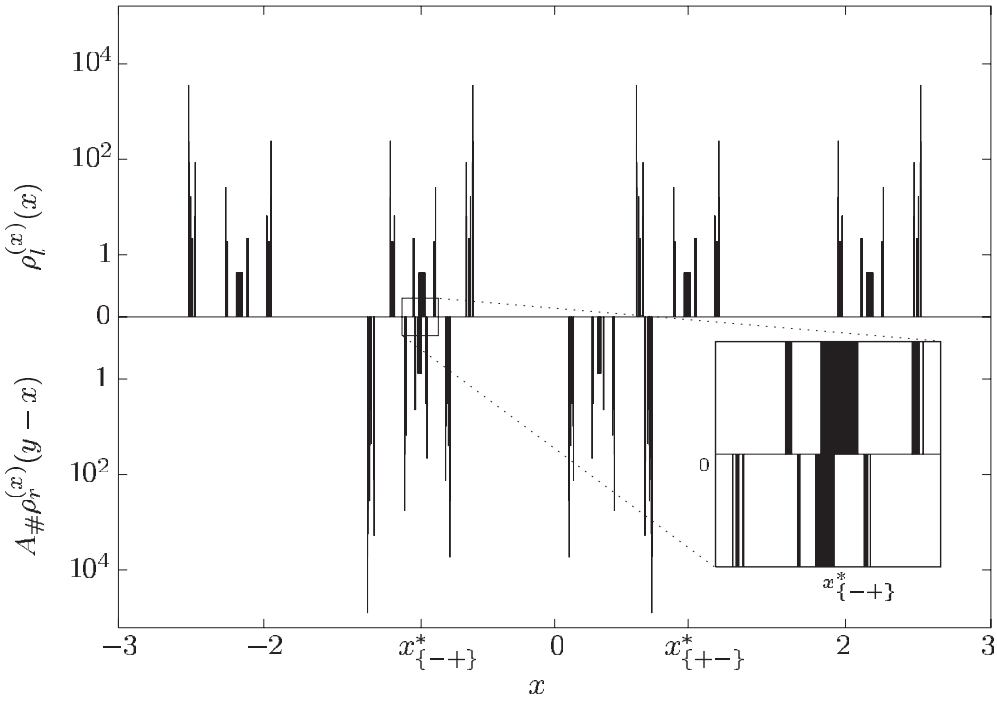

Figure 8. Illustration of the situation leading to the weakest band in the convolution of $\mu_l^{(x)}$ and $A_\#\mu_r^{(x)}$ at $h = 1.54$ and $l = r = 6$. The integration over the product of $\rho_l^{(x)}$ (the density of $\mu_l^{(x)}(x)$, upper part) and $A_\#\rho_r^{(x)}(y-x)$ (the density of $A_\#\mu_r^{(x)}$, lower part) yields the density of the convolution at y. In this figure $y = 0.309\,965$ which is the position of the weakest band. Only for the weak band around $x^*_{\{-+\}}$ the are two densities simultaneously non-zero (see inset). This leads to a very small value for the density of the convolution. Note that even though the two convoluted measures are already rather sparse, the convolution still has non-fractal support at this h. $\beta = J = 1$.

different h. For $h \approx 1.5$ there is a relative position for the approximations $\mu_l^{(x)}$ and $A_\#\mu_r^{(x)}$ for which only the two very weak bands around x^*_{+-} and $A(x^*_{+-})$ overlap, leading to a very weak band in the convolution (cf figure 8 for an example). This results in the large values of D_q we observe numerically for the iteration depths $l = r \leqslant 10$. For $h \approx 1.6$ the band structure is of a form such that no such position can be found in the iteration depths under consideration. For any relative position of the two approximations of the measures more than one pair of bands or considerably stronger ones overlap. This results in the considerably smaller values of D_q. For larger h the formation of a very weak band in the convolution reappears and we again obtain large values of D_q ($q < 0$). For other iteration depths the situation can again change as there is no strict self-similarity of the measure $\mu^{(m)}$. From another point of view for a given iteration depth the values of D_q strongly depend on the random field strength h due to similar changes in the overlap structure as discussed so far. We expect that on any iteration depth this situation is qualitatively the same.

6. Conclusions

In order to investigate the multifractal properties of the measure of the local magnetization in the random-field Ising chain we studied the relation between the multifractal properties of two

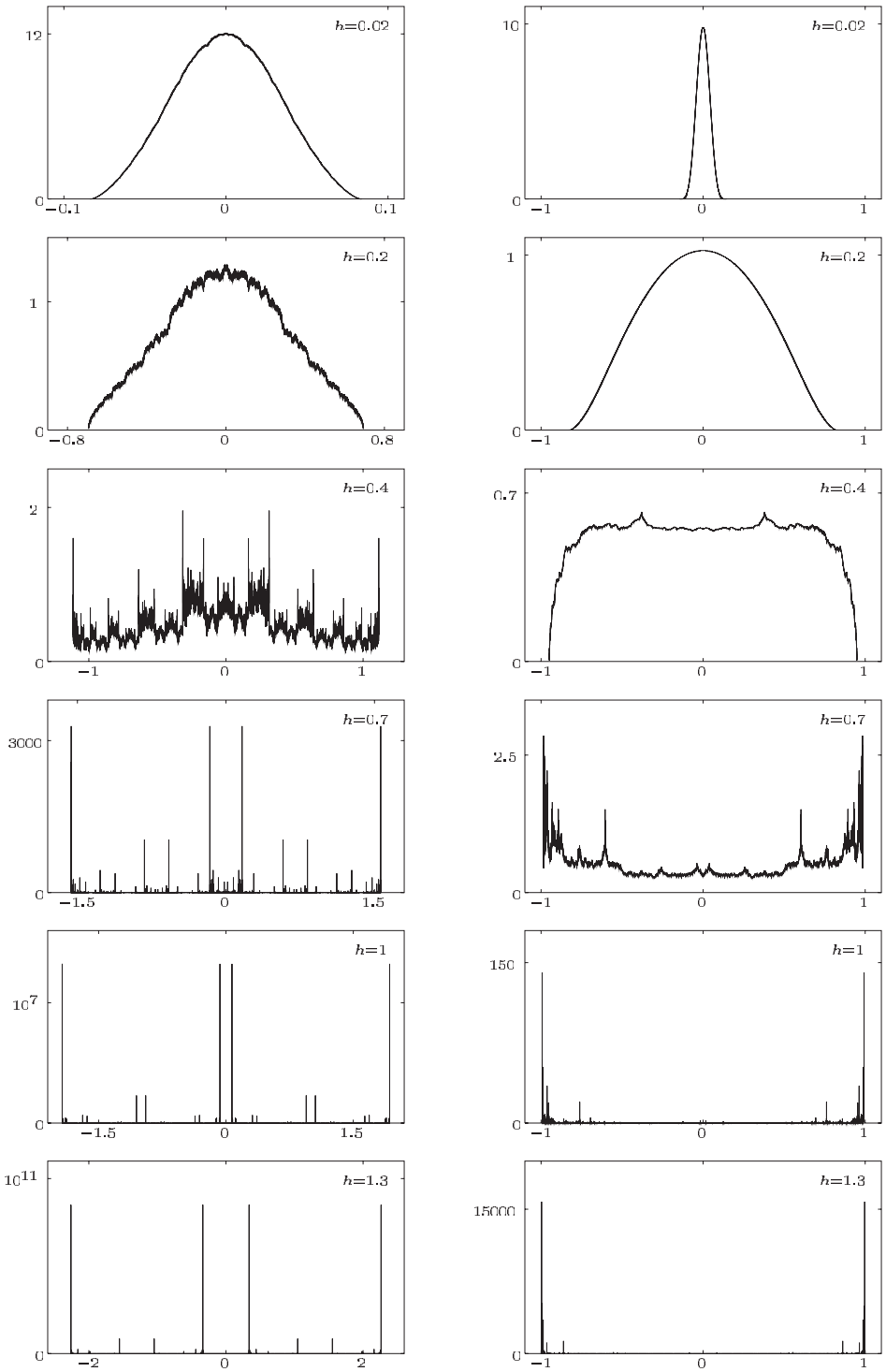

Figure 9. Measure densities of the effective field (left column) for iteration depth 16 and the local magnetization (right column) for iteration depth $l = r = 8$. The details are explained in the text. $\beta = J = 1$.

measures and their convolution. The pointwise dimension at the boundary of the support of the convolution turned out to be the sum of the pointwise dimensions at the boundary of the two measures. This enabled us to calculate the pointwise dimension at the boundary of the support of the measure of the local magnetization and employ this to give bounds on the D_q-spectrum.

We furthermore were able to prove that the generalized dimensions D_q of the convolution are bounded from above by the sum of the D_q of the two convoluted measures. This yields upper bounds on the D_q-spectrum of the measure of the local magnetization.

The general results were illustrated for the convolution of Cantor sets with weights and our main application, the measure of the local magnetization in the random-field Ising model. We also performed numerical studies of the D_q-spectra employing a box method and a method based on a new natural partition. The numerical data are consistent with the exact inequalities but reveal a complicated structure for the D_q-spectrum of the measure of the local magnetization for $q < 0$ and $1.2 \lesssim h \lesssim 1.7$. The numerical instability of the method based on the new natural partition in this region can be understood by analysing the band structure of the approximations of the invariant measure of the effective field. Nevertheless, it prevents us from obtaining the asymptotic scaling. We therefore took a pragmatic approach and investigated what an experimentalist could possibly hope to observe, resulting in the shown D_q-estimates based on the box method.

Investigating the probability measure of the local magnetization of the one-dimensional random-field Ising model we for the first time considered a physical quantity which in principle is measurable. Furthermore, the general results about convolutions of multifractal measures can be of interest in other areas as well, as it is not unusual that sums of random variables appear.

All figures were presented for a generic choice of parameters, $\beta = J = 1$. The behaviour for $\beta, J \to 0$ and $\beta, J \to \infty$ is more or less trivial. For $\beta \to 0$ the probability measure of the local magnetization is a Dirac measure at 0. For $J \to 0$ it is the sum of two Dirac measures at $\pm \tanh \beta h$. In the limit $\beta \to \infty$ the distribution of the effective field is a finite sum of Dirac measures [5,6] and therefore the measure of the local magnetization is also such a sum. Finally, in the unphysical limit $J \to \infty$ the function $A(x)$ is the identity, $A(x) = x$, and the RIFS for the effective field therefore ceases to be contractive. The measures μ_n of the effective field for finite system sizes need not converge in the Hutchinson metric in the thermodynamic limit $n \to \infty$. The proof for existence and uniqueness of the convolution of lemma 3.1 therefore does not apply. One needs to consider finite systems and take the thermodynamic limit in the end. The RIFS is a symmetric random walk with step size h and the local magnetization is $m_{l,r} = \tanh \beta(x_l + y_r)$ where x_l and y_r are two random walks of length l and r respectively. Thus, $1/\beta \operatorname{artanh} m_{l,r}$ is also a random walk of length $n = l + r$. One therefore can deduce that the probability for the local magnetization to take values in any closed interval $X \subset [-1, 1]$ tends to zero in the thermodynamic limit $n \to \infty$ because this corresponds to the probability for the random walk to stay in a finite region. The measure of the local magnetization thus converges to the sum of two Dirac measures at ± 1 in the weak topology of Borel measures. In all cases no multifractal effects of interest can be observed.

As a byproduct of our numerical algorithm we can easily produce the measure density of the local magnetization itself (cf figure 9). In the figure we show the measure density $\rho^{(x)}$ of the effective field and the measure density $\rho^{(m)}$ of the local magnetization for some values of the random field strength h. One can clearly see that $\rho^{(m)}$ is much smoother than $\rho^{(x)}$ in accordance with the general belief. For $h = 0.02$ both measures are smooth and the slope at the boundary is zero. For $h = 0.2 > h_c^{(4)}$ the slope of $\rho^{(x)}$ is already infinite whereas the slope of $\rho^{(m)}$ remains zero. For $h = 0.4 > h_c^{(3)} = h_c^{(m,4)}$ the density $\rho^{(x)}$ is infinite at the boundary whereas $\rho^{(m)}$ is zero but has infinite slope. For $h = 0.7 > h_c^{(m,3)}$ the density $\rho^{(m)}$ also is infinite at the boundary. The fractality of the support is in the same way 'delayed' for

$\rho^{(m)}$. For $h = 1.0 > h_c^{(1)}$ the support of $\rho^{(x)}$ is already fractal but the support of $\rho^{(m)}$ is still Euclidean.

Overall, there is a gradual transition from a monomodal strongly peaked distribution for small random field to an even more strongly peaked bimodal distribution for large random field. The local magnetization (which is a thermo-dynamic average but still a random variable with respect to the probability space of the random field) shows a transition from a paramagnetic situation where the most probable value is zero to a ferromagnetic situation where the most probable value is ± 1. Between these extremal situations lies the multifractal regime. The distribution always remains symmetric such that this is not a phase transition; there is no symmetry breaking even if a small homogeneous field is applied.

Appendix

Let $x_i = i\varepsilon$, $I \in \mathbb{Z}$ and $x_i' = x_i + y$, $i \in \mathbb{Z}$ be two grids which are shifted by y with respect to each other and let $q > 0$. In this appendix we show that

$$\sum_i \mu(B_{\frac{\varepsilon}{2}}(x_i'))^q \leqslant 2^{q+1} \sum_i \mu(B_{\frac{\varepsilon}{2}}(x_i))^q. \tag{A.1}$$

Let $i \in \mathbb{Z}$ and denote $\mu_i := \mu(B_{\frac{\varepsilon}{2}}(x_i))$ and $\mu_i' := \mu(B_{\frac{\varepsilon}{2}}(x_i'))$. Clearly, $\mu_i' \leqslant \sum_{j \in J(i)} \mu_j$ where $J(i) = \{j \in \mathbb{Z} : B_{\frac{\varepsilon}{2}}(x_j) \cap B_{\frac{\varepsilon}{2}}(x_i') \neq \emptyset\}$. As $B_{\frac{\varepsilon}{2}}(x_i')$ intersects at most two $B_{\frac{\varepsilon}{2}}(x_j)$ the set $J(i)$ has at most two elements and we can write

$$\mu_i'^q \leqslant 2^q \max_{j \in J(i)} \mu_j^q. \tag{A.2}$$

On the other hand each $B_{\frac{\varepsilon}{2}}(x_j)$ intersects at most two $B_{\frac{\varepsilon}{2}}(x_i)$ for a fixed j such that μ_j appears at most twice when summing (A.2) over all i. Therefore,

$$\sum_i \mu_i'^q \leqslant 2 \cdot 2^q \sum_i \mu_i^q \tag{A.3}$$

which is the result claimed in (A.1).

References

[1] Bruinsma R and Aeppli G 1983 *Phys. Rev. Lett.* **50** 1494
Bruinsma R and Aeppli G 1983 *Phys. Lett.* A **97** 117
[2] Normand J M, Mehta M L and Orland H 1985 *J. Phys. A: Math. Gen.* **18** 621
[3] Andelman D 1986 *Phys. Rev.* B **34** 6214
[4] Györgyi G and Ruján P 1984 *J. Phys. C: Solid State Phys.* **17** 4207
[5] Behn U and Zagrebnov V A 1987 JINR E 17-87-138 Dubna
[6] Behn U and Zagrebnov V A 1988 *J. Phys. A: Math. Gen.* **21** 2151
[7] Behn U and Zagrebnov V A 1987 *J. Stat. Phys.* **47** 939
[8] Szépfalusy P and Behn U 1987 *Z. Phys.* B **65** 337
[9] Nowotny T, Patzlaff H and Behn U 2001 *J. Phys. A: Math. Gen.* **34** 1
[10] Ruján P 1978 *Physica* A **91** 549
[11] Behn U and Lange A 1992 *From Phase Transitions to Chaos* ed G Györgyi, I Kondor, L Sasvári and T Tél (Singapore: World Scientific) p 217
[12] Patzlaff H, Behn U and Lange A 1997 *Fractal Frontiers, Fractals in the Natural and Applied Sciences* ed M M Novak and T G Dewey (Singapore: World Scientific) p 95
[13] Evangelou S N 1987 *J. Phys. C: Solid State Phys.* **20** L511
[14] Bene J and Szépfalusy P 1988 *Phys. Rev.* A **37** 1703
[15] Bene J 1989 *Phys. Rev.* A **39** 2090
[16] Behn U, van Hemmen J L, Kühn R, Lange A and Zagrebnov V A 1994 *On Three Levels* ed M Fannes *et al* (New York: Plenum) p 399
[17] Bleher P M, Ruiz J and Zagrebnov V A 1996 *J. Stat. Phys.* **84** 1077

[18] Behn U, Priezzhev V B and Zagrebnov V A 1990 *Physica* A **167** 481
[19] Luck J M and Nieuwenhuizen Th M 1989 *J. Phys. A: Math. Gen.* **22** 2151
[20] Nieuwenhuizen Th M and Luck J M 1986 *J. Phys. A: Math. Gen.* **19** 1207
[21] Derrida B, Vannimenus J and Pomeau Y 1978 *J. Phys. C: Solid State Phys.* **11** 4749
[22] Tanaka T, Fujisaka H and Inoue M 1989 *Phys. Rev.* A **39** 3170
[23] Tanaka T, Fujisaka H and Inoue M 1990 *Prog. Theor. Phys.* **84** 584
[24] Schmidt H 1957 *Phys. Rev.* **105** 425
[25] Halperin B I 1967 *Adv. Chem. Phys.* **13** 123
[26] Barnes C and Luck J M 1990 *J. Phys. A: Math. Gen.* **23** 1717
[27] Luck J M 1992 *Systèmes Desordonnés Unidimensionnels* ed C Godreche (Paris: Collection Alea-Saclay)
[28] Ledrappier F and Porzio A 1994 *J. Stat. Phys.* **76** 1307
Ledrappier F and Porzio A 1996 *J. Stat. Phys.* **82** 367
Ledrappier F and Porzio A 1996 *J. Stat. Phys.* **82** 397
[29] van Hemmen J L, Keller G and Kühn R 1988 *Europhys. Lett.* **5** 663
[30] Behn U, van Hemmen J L, Kühn R, Lange A and Zagrebnov V A 1993 *Physica* D **68** 401
[31] Radons G, Schuster H G and Werner D 1993 *Phys. Lett.* A **174** 293
[32] Hutchinson J E 1981 *Indiana Univ. Math. J.* **30** 713
[33] Radons G 1992 *J. Stat. Phys.* **72** 227
[34] Falconer K J and O'Neil T C 1999 *Math. Nachr.* **204** 61
[35] Radons G 1995 *Phys. Rev. Lett.* **75** 2518
[36] Radons G and Stoop R 1996 *J. Stat. Phys.* **82** 1063
[37] Stoop R and Steeb F-H 1997 *Phys. Rev.* E **55** 6589
[38] de la Torre A C, Maltz A, Mártin H O, Catuogno P and García-Mata I 2000 *Phys. Rev.* E **62** 7748
[39] Belanger D P 1998 *Spin Glasses and Random Fields* ed A P Young (Singapore: World Scientific) p 251
[40] Riedi R 1995 *J. Math. Anal. Appl.* **189** 462
[41] Bauer H 1990 *Maß und Integrationtheorie* (Berlin: de Gruyter)
[42] Halsey T C, Jensen M H, Procaccia I and Shraiman B I 1989 *Phys. Rev.* A **33** 1141